ISSN 0020-4412, Instruments and Experimental Techniques, 2008, Vol. 51, No. 4, pp. 511–522. © Pleiades Publishing, Ltd., 2008.
Original Russian Text © A.V. Aref'ev, I.M. Belyaev, B.M. Bobchenko, K.I. Voronchev, A.I. Golutvin, O.B. Gushchin, V.Yu. Egorychev, I.E. Korol'ko, T.G. Kvaratskheliya, I.V. Machikhil'yan, M.S. Prukudin, V.Yu. Rusinov, D.V. Rusinov, E.I. Tarkovskii, Yu.V. Gilitskii, S.Ya. Barsuk, S.V. Shuvalov, 2008, published in Pribory i Tekhnika Eksperimenta, 2008, No. 4, pp. 25–37.

NUCLEAR EXPERIMENTAL TECHNIQUES

A Study of Light Collection in "Shashlik" Calorimeters

A. V. Aref'ev[a], I. M. Belyaev[a], B. M. Bobchenko[a], K. I. Voronchev[a], A. I. Golutvin[a], O. B. Gushchin[a], V. Yu. Egorychev[a], I. E. Korol'ko[a], T. G. Kvaratskheliya[a], I. V. Machikhil'yan[a], M. S. Prukudin[a], V. Yu. Rusinov[a], D. V. Rusinov[a], E. I. Tarkovskii[a], Yu. V. Gilitskii[b], S. Ya. Barsuk[c], and S. V. Shuvalov[d]

[a] *Alikhanov Institute for Theoretical and Experimental Physics, ul. Bol'shaya Cheremushkinskaya 25, Moscow, 117218 Russia*
[b] *Institute for High Energy Physics, ul. Pobedy 1, Protvino, Moscow oblast, 142281 Russia*
[c] *Laboratoire de l'Accelerateur Lineaire, Université Paris-Sud, 11, Bat 200, 91898, Orsay cedex, Paris, France*
[d] *Deutsches Elektronen-Synchrotron, Platanenalle 6 D-15738, Zeuthen, Germany*

Received January 28, 2008

Abstract—The spatial nonuniformities of the response and the absolute light yield in calorimeter modules with interleaved absorber and scintillator layers were investigated on high-energy muon and electron beams. A program for detailed simulation of light collection in scintillator tiles of the calorimeter using the Monte Carlo method was developed to describe the whole set of experimental results. The experimental data are in good agreement with the results of simulation.

PACS numbers: 29.40.Vj, 42.15.Dp

DOI: 10.1134/S0020441208040040

1. INTRODUCTION

Ignoring electronic noise, the energy resolution of an electromagnetic calorimeter is

$$\frac{dE}{E} = \frac{a}{\sqrt{E}} \oplus b, \qquad (1)$$

where a is the sampling term and b is the constant term in the calorimeter resolution; sign $\oplus$ denotes quadratic addition. For sampling calorimeters with a sufficiently high light yield, the sampling term is governed by the thickness of the absorber plates. The Moliere radius describing the transverse dimensions of an electromagnetic shower is the other important parameter of an electromagnetic calorimeter. In a calorimeter with a small Moliere radius, the electron and photon energies can be reconstructed by adding the signals from fewer cells, which substantially improves the efficiency of reconstruction at high occupancies.

To produce a calorimeter with a high energy resolution and a small Moliere radius (i.e., with a high ratio of the absorber and scintillator thicknesses), one must use thin lead plates and the thinnest possible scintillator tiles. A decrease in the thickness of scintillator tiles, along with a decrease in the light yield, leads to an increase in the spatial nonuniformity of light collection and thereby to degradation in the energy resolution, caused by an increase in fixed term b in Eq. (1). Therefore, for further progress in development of calorimeters with interleaved lead and scintillator layers, it is necessary that

—the ratio of thicknesses of the lead absorber and scintillator plates be optimized in view of the physical problems and conditions of a particular experiment;

—a technology for manufacturing thin (0.5 mm or less) scintillator tiles be developed; and

—methods for improving the homogeneity of light collection in thin scintillator tiles be devised.

To study light collection processes in scintillator tiles, the nonuniformity of the responses of LHCb electromagnetic calorimeter modules [1] and an experimental calorimeter module (hereinafter referred to as the experimental module) with 0.5-mm-thick lead and scintillator plates was measured with high-energy muon and electron beams. The absolute light yields in these modules were additionally measured. A program for simulating light propagation processes in scintillator tiles was developed to interpret the whole set of experimental data and determine the optical parameters that were thought most critical for attaining uniform light collection. The main optical parameters of the module were found by comparing the measured nonuniformity of the response to the simulation results.

When comparing the experimental and theoretical data, the calculations additionally took into account the variation of the scintillator tile thickness and the distribution of the energy deposited by particles in the calorimetric assembly, calculated with the aid of simulation based on the GEANT code [2, 3]. The parameters of the mathematical model obtained thereby were used to find the relative values of the light yield in the inner, middle, and outer modules of the LHCb calorimeter [1], as well as in the experimental module. The results of simula-

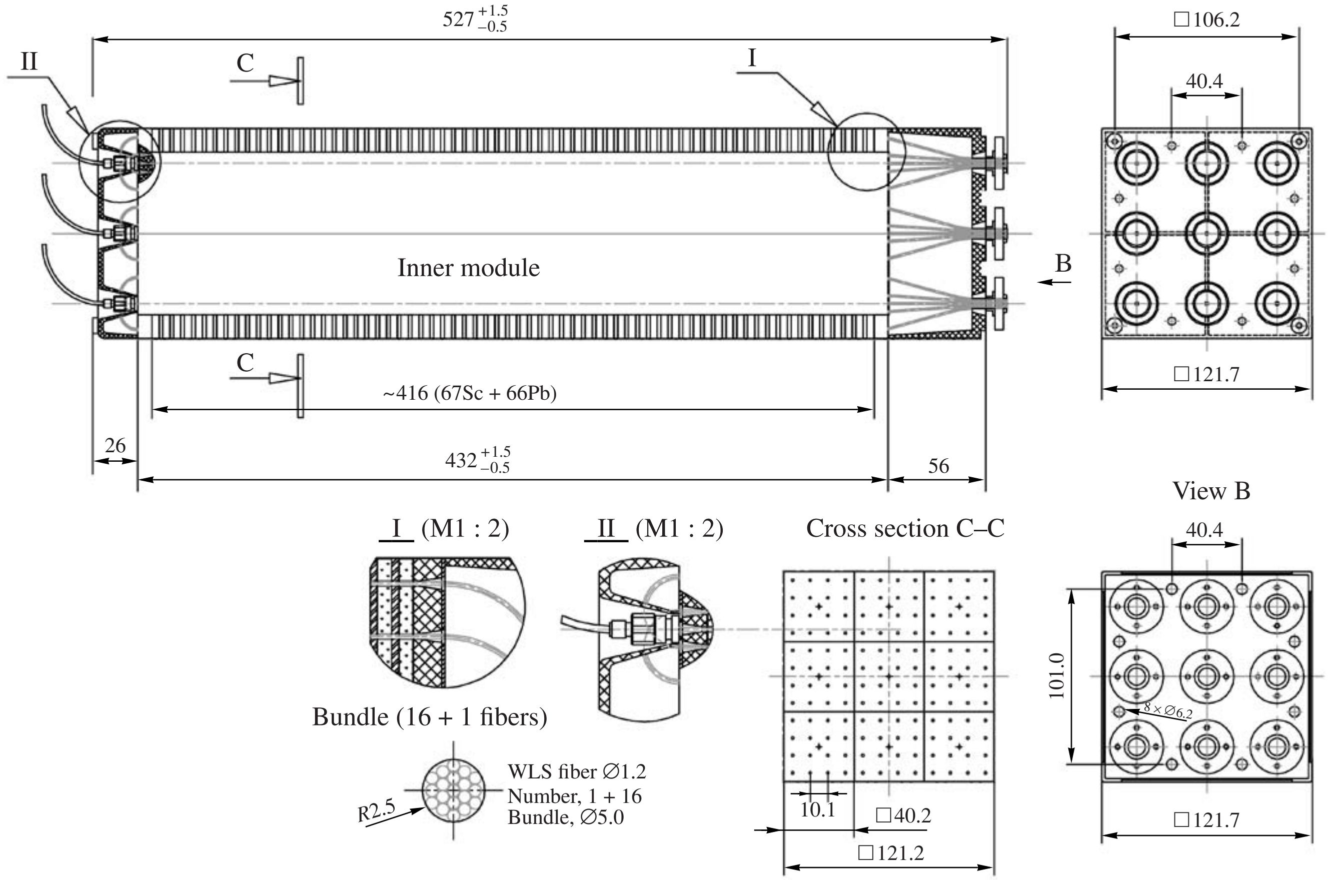

Fig. 1. Inner module of the LHCb calorimeter.

tion were compared to the results of measurements both on the particle beams and on the test bench that detected cosmic muons.

2. EXPERIMENT

2.1. Description of the Setup

The nonuniformity of the response of calorimeter modules was measured on the SPS CERN accelerator on the X7B secondary particle beam [4]. The measurements were taken with 100-GeV muons and 50-GeV electrons. The cross section of the secondary beams was 10×30 mm^2 for electrons and 30×30 mm^2 for muons.

The calorimetric assembly was composed of nine modules that formed an array of 3×3. The module being tested was placed at the center of the assembly, while the peripheral modules were used to measure the transverse energy leakage.

The transverse dimensions of the LHCb calorimeter module were 121×121 mm^2. The module (Fig. 1) consisted of alternating layers of 2-mm-thick lead and 4-mm-thick polystyrene-based scintillator. The lead and scintillator layers were interleaved with thin sheets of a special white paper—DuPont Tyvek®—0.12 mm thick to exclude optical contact between the lead and the scintillator and maintain diffuse reflection of light that leaves the scintillator. A stack of lead and scintillator layers was placed between two steel plates 1 mm thick. Four 0.1-mm-thick steel straps were welded to the ends of these plates. Such a design ensured mechanical strength of the module. Scintillator tiles of the middle and inner modules of the LHCb calorimeter were divided, respectively, into four and nine light-isolated cells of uniform size. In the middle module, the dimensions of the cell were 60×60 mm^2; in the inner module, 40×40 mm^2. A 0.1-mm-thick white coating providing diffuse reflection was formed at the end surfaces and a thin border near the edges of each scintillator tile by chemical etching of it.

Y11 wavelength-shifting fibers (Kuraray) were inserted in holes drilled in the modules. Wavelength-shifting (WLS) fibers were located at the nodes of a grid with cells of 15×15 mm^2 for the outer modules and 10×10 mm^2 for the inner and middle modules of the LHCb calorimeter. The outer module was pierced by 64 WLS fibers; the middle module, by 36 fibers per each of the four light-isolated cells; the inner module, by 16 fibers per each of the nine light-isolated cells. The WLS fiber has a radius of 0.6 mm and consists of two

Table 1. Geometrical parameters of the modules

Parameters	Outer module	Middle module	Inner module	Experimental module
Number of layers (lead/scintillator)	66/67	66/67	66/67	280/280
Layer thickness (lead/scintillator), mm	2/4	2/4	2/4	0.5/0.5
Dimensions of the cell, mm^2	121×121	60×60	40×40	40×40
Cells per module	1	4	9	9
Number of WLS fibers in a cell	64	36	16	16
Separation between the WLS fibers, mm	15	10	10	10

transparent claddings with refractive indices of 1.42 and 1.49 and a WLS core with a refractive index of 1.59, which reemits scintillation light and transmits the major portion of it over the fiber by total internal reflection. The thickness of each transparent cladding is 0.036 mm.

At the center of each light-isolated cell, there were holes for clear fibers used to transport light from the optical fibers of the monitoring system to photomultiplier tubes (PMTs). On the rear side of the module, fibers corresponding to each individual light-isolated cell were joined in a bundle. The fiber tips in each bundle were polished. Light from each fiber bundle was transmitted to a rectangular polystyrene parallelepiped, which uniformly distributed the light over the photocathode surface to eliminate the effect of the photocathode inhomogeneity.

The experimental module was composed of 280 0.5-mm-thick lead layers and 280 0.5-mm-thick scintillator layers. The edges of the scintillator tiles used in the module did not have a matte border. In all other respects, the experimental module was similar in design to the inner module of the LHCb calorimeter. The geometrical parameters of all modules subjected to tests are presented in Table 1.

The stability of the performance characteristics of the test calorimetric assembly was monitored with the aid of the monitoring system based on two LEDs, one of which was used to illuminate the outer modules of the assembly and the other illuminated the tested module. The brightness of LED flashes was checked by means of a high-stability PIN diode. The LEDs were fired by an external pulser, which successively triggered the LEDs and the system for reading out the setup parameters in order to monitor the pedestal positions and widths.

The entire calorimetric assembly was disposed on a mobile platform capable of changing the position of the assembly with respect to the beam. The accuracy in positioning the calorimetric assembly was ±1 mm.

2.2. Coordinate Measurements

Three delay wire chambers [5] were used to measure the coordinate of the point of particle incidence onto the calorimeter module (Fig. 2). Each track was approximated by a straight line:

$$x = \alpha_x + \beta_x z; \quad y = \alpha_y + \beta_y z.$$

Parameters α and β were obtained by minimizing χ^2:

$$\chi_x^2 = \sum_{i=1}^{3} \frac{((\alpha_x + \beta_x z_i) - x_i)^2}{\delta^2},$$

where z_i is the distance between the calorimetric assembly and the ith chamber, and $\delta = 0.2$ mm [5].

A similar formula was also used to determine the second coordinate. Tracks with $\chi^2 > 4$ were rejected. The distribution of distances between the reconstructed track and the measured coordinate in the final chamber is shown in Fig. 3.

The design features of the calorimeter modules were used to check the validity of reconstructed coordinates. The detector response to muons with trajectories the major portion of which passes either outside the scintil-

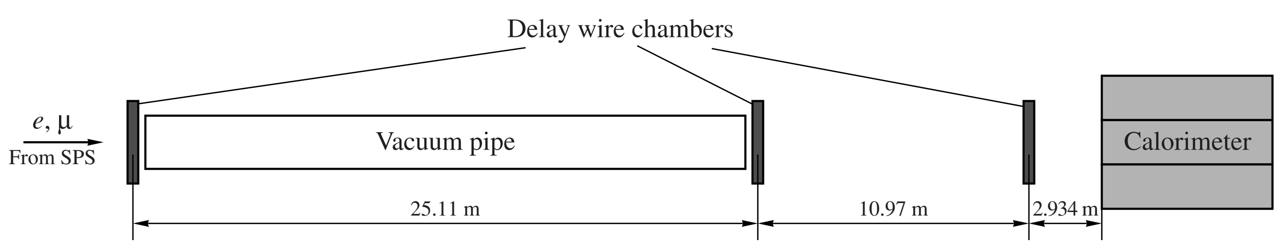

Fig. 2. Layout of the delay wire chambers and the test calorimetric assembly.

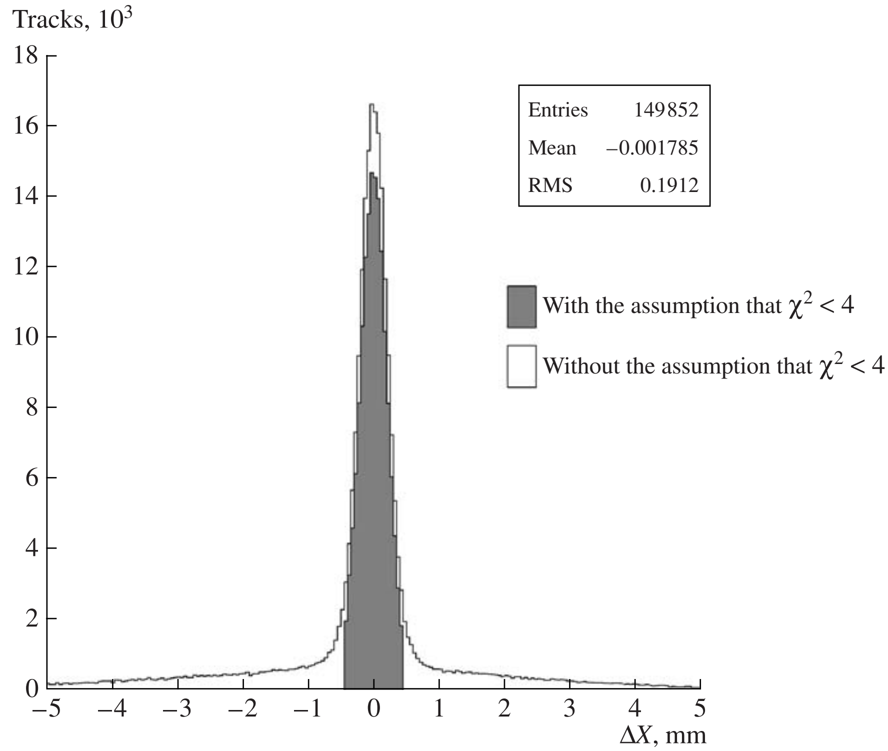

Fig. 3. Difference between the coordinate measured by the closest to the calorimeter delay wire chamber and the reconstructed particle track.

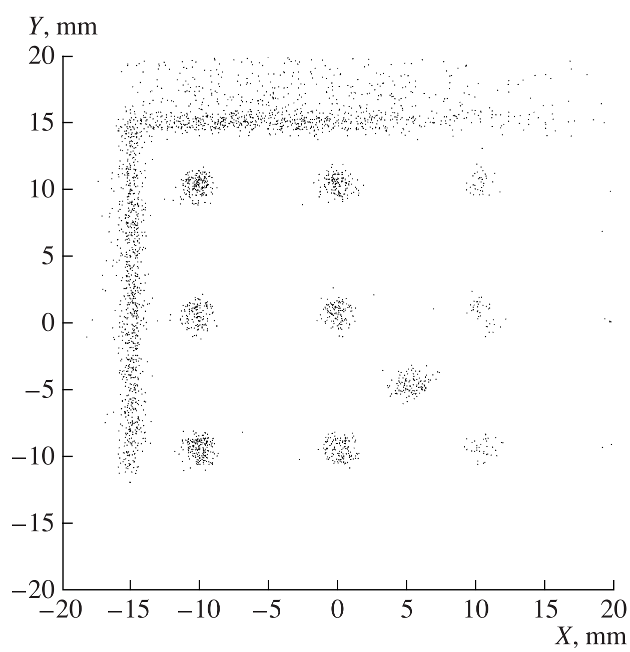

Fig. 4. Distribution of the coordinates of 100-GeV muon hit points, provided that the energy deposited in the cell was 60–65% of the most probable value of the Landau function approximating the energy deposited in the calorimeter. Dots correspond to muons with trajectories crossing only a part of the scintillator tiles in the cell selected.

lator tiles of a particular cell or inside the holes in these tiles is substantially lower than the response to a muon traveling through all scintillator layers. We selected muons for which the response was 60–65% of the maximum value of the Landau function approximating the muon signal in the entire calorimetric cell. For muons selected thereby, the distribution of the coordinates of their hit points was plotted. Clusters of points in this distribution (Fig. 4) correspond to the boundaries between adjacent light-isolated cells and the holes in the calorimeter module.

2.3. Measuring the Nonuniformity of the Calorimeter Response

The transverse dimensions of cells in the calorimeter modules are substantially greater than the particle beam size. To cover the whole area of the calorimeter cell, measurements were taken for different positions of the module relative to the beam. Distributions similar to the map in Fig. 4 were plotted for each position of the tested assembly with respect to the beam. A constant coefficient was added to (or subtracted from) the coordinate in each position, so that the central hole of the cell under investigation had coordinates (0, 0) and the coordinates of holes observed in several positions of the assembly coincided. As a result, coordinates of the particle's point of incidence onto the calorimeter module were referred to a unified coordinate system (see

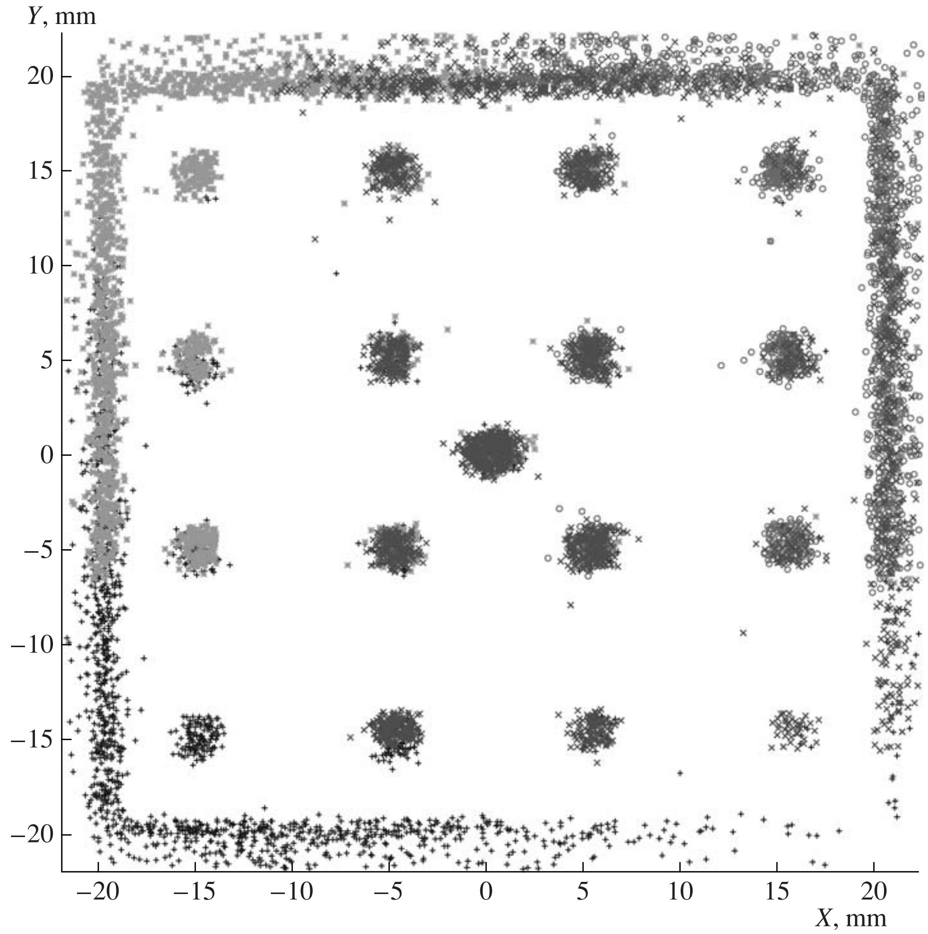

Fig. 5. Distribution of the coordinates of muon hit points for different positions (different symbols of dots) of the calorimetric assembly with respect to the beam, provided that the energy deposited in the cell was 60–65% of the most probable value of the Landau function approximating the energy deposited in the calorimeter. Dots correspond to muons with trajectories crossing only a part of the scintillator tiles in the cell selected.

Fig. 5). In this case, the accuracy in determining the coordinates of hit points of particles incident on the calorimeter module was 0.25 mm. A similar procedure was used in measurements with the electron beam.

To obtain the map of nonuniformities for muons, the dependence of the calorimeter response on the coordinate of the muon’s point of incidence on the central cell of the central module in the calorimeter assembly was investigated. The energy deposited in the cell under investigation only was taken into account when determining the muon signal. The surface of this cell was divided into squares of 1×1 mm^2, and an individual distribution over the muon signal energy was constructed for each square. The distributions obtained thereby were fitted with the Landau function, as is shown in Fig. 6a. The positions of the most probable value in these distributions, plotted on a two-dimensional histogram, provided a map of the nonuniformity of the calorimeter response to muons. The nonuniformity of the response was examined with the aid of muons according to the described procedure for all types of modules. For the outer module, the size of the signal collection area was 1×2 mm^2 due to statistical limitation of the experimental data. (Some results will be presented in Section 4.)

In measurements with the electron beam, the response of each module in the assembly was preliminarily calibrated using electron beams with energies of 100 and 20 GeV. The maps of the calorimeter response nonuniformity were obtained for 50-GeV electrons. The electron signal was determined as a sum of the energies deposited in all cells of the central module of the assembly and four outer modules, which were disposed crosswise with respect to the central one and bordered it on their sides. The leaks into the corner modules of the assembly were negligible and, hence, were ignored when calculating the energy. The surface of the cell under investigation was divided into squares of 1×1 mm^2, for each of which an individual distribution of the electron signal was plotted. These distributions were fitted with the Gaussian function, as is shown in Fig. 6b. The positions of maxima in these distributions,

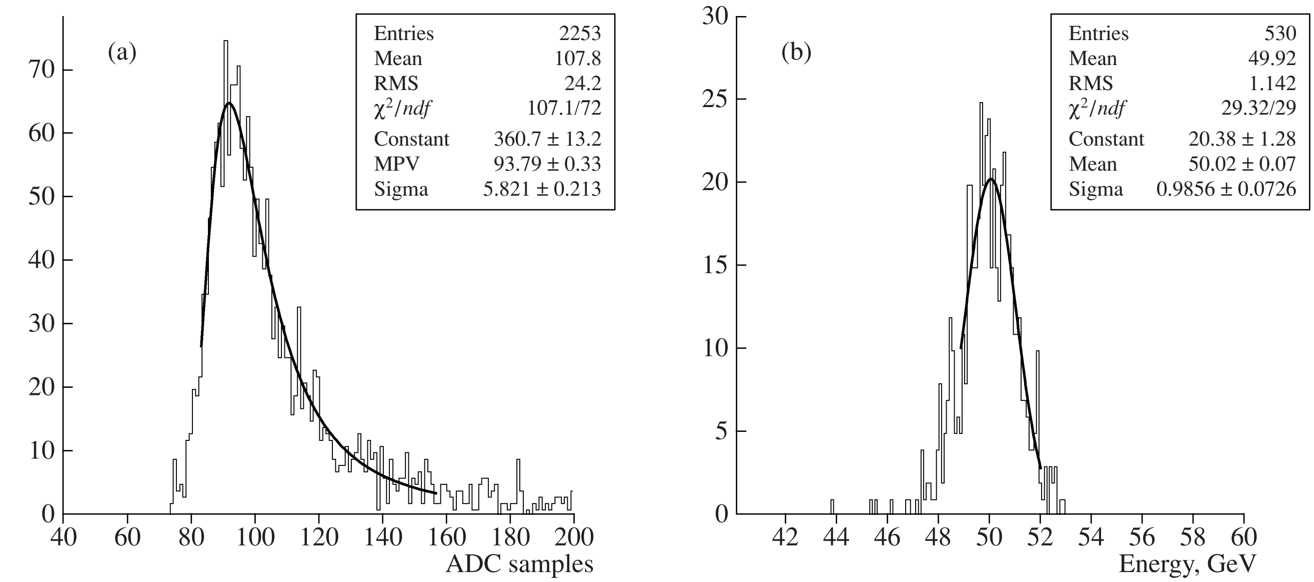

Fig. 6. Examples of the fitted distributions (a) for muons and (b) for electrons. Curves correspond to the fits by the Gaussian and Landau curves for electrons and muons, respectively.

plotted on a two-dimensional histogram, provided a map of the calorimeter response nonuniformity for electrons. (Some results will be presented in Section 4.)

2.4. Measuring Light Yield in the Calorimeter

The light yield was measured with the aid of the monitoring system. For small signals (<500 photoelectrons), the width of the monitoring signal was determined by photoelectron statistics, i.e., by fluctuations of photoelectrons produced at the PMT photocathode by each light flash. In this case, the mean number of photoelectrons can be calculated according to the formula (with the dispersion of the dynode system gain being ignored)

$$N = (A_{LED}/\delta_{LED})^2,$$

where A_{LED} is the measured amplitude of the LED signal and δ_{LED} is its Gaussian width.

The pedestal width was quadratically subtracted from the width of the LED signal. Any systematic error may cause only broadening of the signal, which will result in underestimation of the light yield. Therefore, a set of measurements with different amplitudes of the LED firing signal was performed for each module. It was shown that, in a certain range of amplitudes, the ratio of the calculated number of photoelectrons to the signal amplitude is independent of the LED signal amplitude and has the maximum value. The data obtained thereby, as well as the light yields in the outer, middle, and inner modules, which were measured on the test bench using cosmic rays, are presented in Table 2.

3. SIMULATING THE NONUNIFORMITY OF THE CALORIMETER RESPONSE

3.1. Program for Simulating Light Collection

Production of one photon in a polyvinyl toluene scintillator requires ~100 eV [6]. (The brightness of a polystyrene-based scintillator is ~30% lower.) Mathematical simulation performed for the LHCb calorimeter modules under investigation using the GEANT software package showed that the incident electron deposits ~16% of its energy in the scintillator. Therefore, 1.1×10^6 photons are produced in the LHCb calorime-

Table 2. Results of simulation and measured light yields in the calorimeter modules

Method for investigating the light yield	Inner LHCb module	Middle LHCb module	Outer LHCb module	Experimental module
Beam tests	3000 ± 150	3600 ± 180	2500 ± 130	700 ± 60
Test bench with cosmic rays	3100 ± 130	3500 ± 170	2600 ± 120	No measurements
Simulation	3000	3600	2570	600

ter per 1 GeV of the incident electron energy. At the same time, a PMT registers ~3000 photoelectrons. Taking onto account the quantum efficiency of the PMT (~17% according to the Hamamatsu data), one can estimate the probability of a photon being transported to the PMT as ~1.0%. Available experimental data on the nonuniformity of the response of the LHCb calorimeter modules to high-energy muons have an accuracy of ~0.5%. For the accuracy of simulation comparable to the experimental accuracy to be attained, the number of simulated photons must be $>4 \times 10^6$ for each square region (with an area of 1×1 mm^2) of a calorimetric cell.

A ray tracing program was developed to simulate light collection in scintillator tiles of the calorimeter. This program was written in C++ language with minimum dependence on external program libraries, which allowed us to extensively use the GRID [7] in our computations. To debug the software package, we took advantage of the possibilities of transmitting intermediate data to the ROOT [8] and visualizing the photon trajectory in a scintillation tile.

Refraction, diffuse and mirror reflection, and attenuation of light in the medium and at the surface were all taken into account in the program.

Probability P_{ref} of light being reflected from the boundary between two media was determined using the Fresnel formulas for nonpolarized light:

$$P_{\text{ref}} = \frac{1}{2}\left(\left(\frac{\sin(\theta_i - \theta_r)}{\sin(\theta_i + \theta_r)}\right)^2 + \left(\frac{\tan(\theta_i - \theta_r)}{\tan(\theta_i + \theta_r)}\right)^2\right),$$

where θ_i and θ_r are the angles of incidence and refraction of light, respectively. Diffuse reflection was simulated as a sum of two competitive processes, one of which was mirror reflection with a probability dependent on the photon’s angle of incidence onto the reflector material (see Fig. 7) and the other was isotropic reflection. Attenuation in the medium was calculated according to the exponential law. Scattering in the medium was ignored. To simulate dispersion, the optical parameters of the media were assumed to be functions of the photon wavelength. In addition, the optical parameters of the surfaces were also dependent on the local coordinates, which allowed us to simulate various light masks applied to the scintillator tile surface, in particular, a matte coating at the tile edges and local shading near WLS fibers.

In the mathematical modeling program, the geometry of a scintillator tile with fibers and Tyvek sheets was represented by simple geometrical shapes and Boolean operations on them. For example, a scintillator tile with holes was simulated by a rectangular parallelepiped with cylinders subtracted from it. The tile surface was divided into squares with dimensions of 0.5×0.5 mm^2. While initializing the program, it was established for each square whether or not it intersected a hole, and all other holes in the tile were sorted according to the distance to them and put on the list. This procedure allowed us to substantially (by 4–16 times) accelerate the simulation process, thus reducing the number of checked holes at each elementary step of the program.

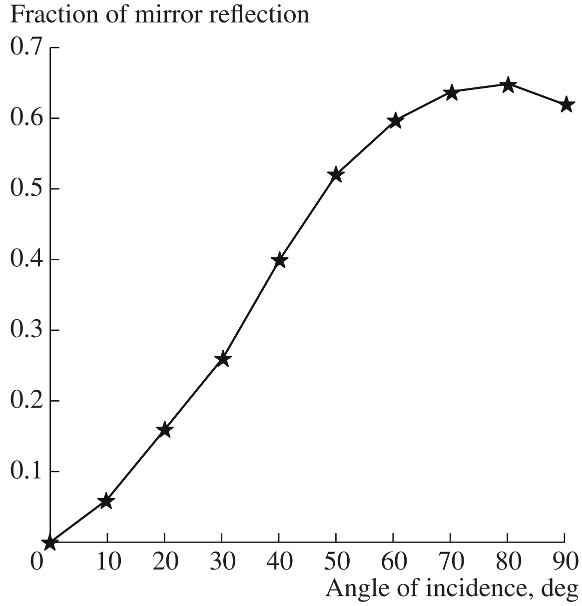

Fig. 7. Fraction of mirror reflection in simulation of diffuse reflection vs. the photon’s angle of incidence.

3.2. Simulating the Scintillator Tile

The geometrical model of the scintillator tile fully complies with its actual configuration. The behavior of the light collection efficiency near the edges of the scintillator tile is governed by the probability of diffuse reflection from the matte coating at the end surfaces and edges of the tile, which is one of the main parameters of the program. This parameter is shown in Fig. 8 versus the wavelength of incident light. In addition, the total probability of diffuse reflection depends on the thickness of the reflective layer. To simulate this dependence, the probability of diffuse reflection was multiplied by a dimensionless coefficient, from now on referred to as the matte coating quality.

The upper and lower surfaces of the tile, except for the border, are transparent for photons with a low probability of diffuse reflection and absorption. Complementing the optical model by processes of diffuse reflection and absorption of a photon in its crossing the transparent boundaries of the scintillator has made it possible to efficiently simulate various defects at the tile surface (scratches, tracks of a press mold, etc.). The numerical value of the total probability of diffuse reflection and absorption, hereinafter referred to as the scintillator surface imperfection, is an important parameter of the optical model. In this case, the ratio of the diffuse reflection and absorption probabilities, which is 2 : 3, is independent of the photon wavelength.

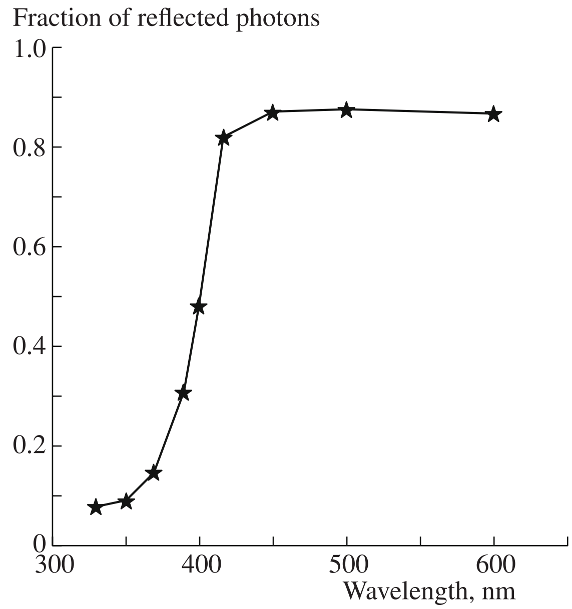

Fig. 8. Probability of diffuse reflection from the matte coating as a function of the photon wavelength.

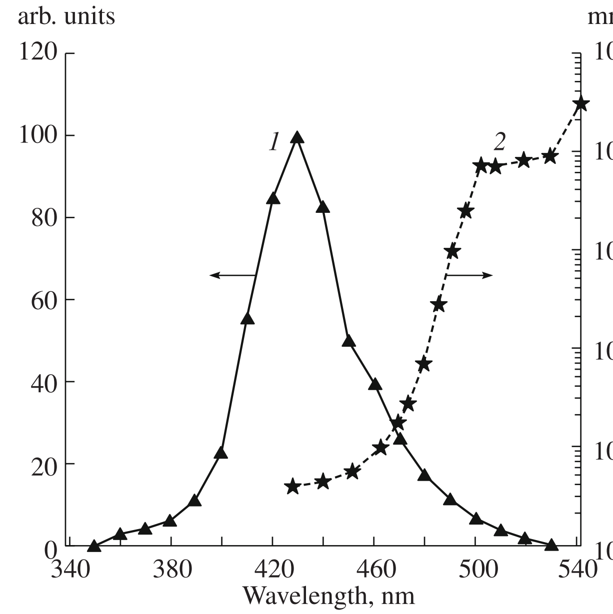

Fig. 9. (*1*) Emission spectrum of the scintillator and (*2*) attenuation length in the core of a WLS fiber.

The refractive index of the scintillator is 1.58. The emission spectrum of the scintillator was simulated in accordance with the data provided by the manufacturer (Fig. 9).

A WLS fiber, the geometrical and optical parameters of which complied with the actual values, was inserted into each hole in the tile. The scintillator tile, together with the WLS fibers, was placed between two layers of Tyvek white paper, in which there were 2-mm-diameter black inserts near each fiber.

To obtain the light collection nonuniformity map, the tile surface was divided into squares of 0.5×0.5 mm^2. The location of the photon production point was simulated uniformly over the area and along the depth inside each square region. The initial directions of photons had an isotropic distribution. Reemission of light in WLS fibers was simulated by selecting a new direction for each photon absorbed in the fiber core. If the direction of a reemitted photon was such that the photon could travel over the fiber suffering total internal reflection in it, this photon was considered to be detected. Inside each square region, 10^7 events of photon production were simulated.

4. COMPARISON OF THE EXPERIMENTAL DATA AND THE RESULTS OF SIMULATION

When comparing the results of simulation to the experimental data, one must take into account variations in the scintillator tile thickness due to the imperfection of the injection molding technology.

The spatial profile of the energy deposited by a particle was simulated using the GEANT3 transport code [2]. At each step of the GEANT code, the local energy deposition in the scintillator was multiplied by the preliminarily calculated efficiency of light collection and the relative tile thickness at this point. This procedure allowed us to obtain only the relative changes in the detector response instead of its absolute value, since it took no account of absolute light yield in the plastic, attenuation of light in the fiber, and PMT quantum efficiency.

The distributions of electron and muon momenta in the GEANT simulation coincided with the measured distributions, while the coordinates of the particle's point of incidence onto the calorimeter were additionally smeared according to the normal distribution with a width of 0.25 mm in order to take into account the spatial resolution of the system of delay wire chambers and multiple scattering. The algorithms used for experimental data processing (for detailed description, see Subsection 2.3) were also employed to analyze the results of GEANT simulation of the test calorimetric assembly. The resulting model maps of the calorimeter response nonuniformity were compared to the maps obtained in the course of beam tests in order to determine the optimum optical parameters of the scintillator tile. In this case, the model maps for the nonuniformity of the response were multiplied by normalization factor n, which was determined using the standard χ^2 minimization procedure:

$$\chi^2 = \sum_{\text{regon}} \frac{(\text{Experiment} - n \times \text{Model})^2}{\text{Error}^2},$$

where the error is the quadratic sum of the experimental and normalized model errors.

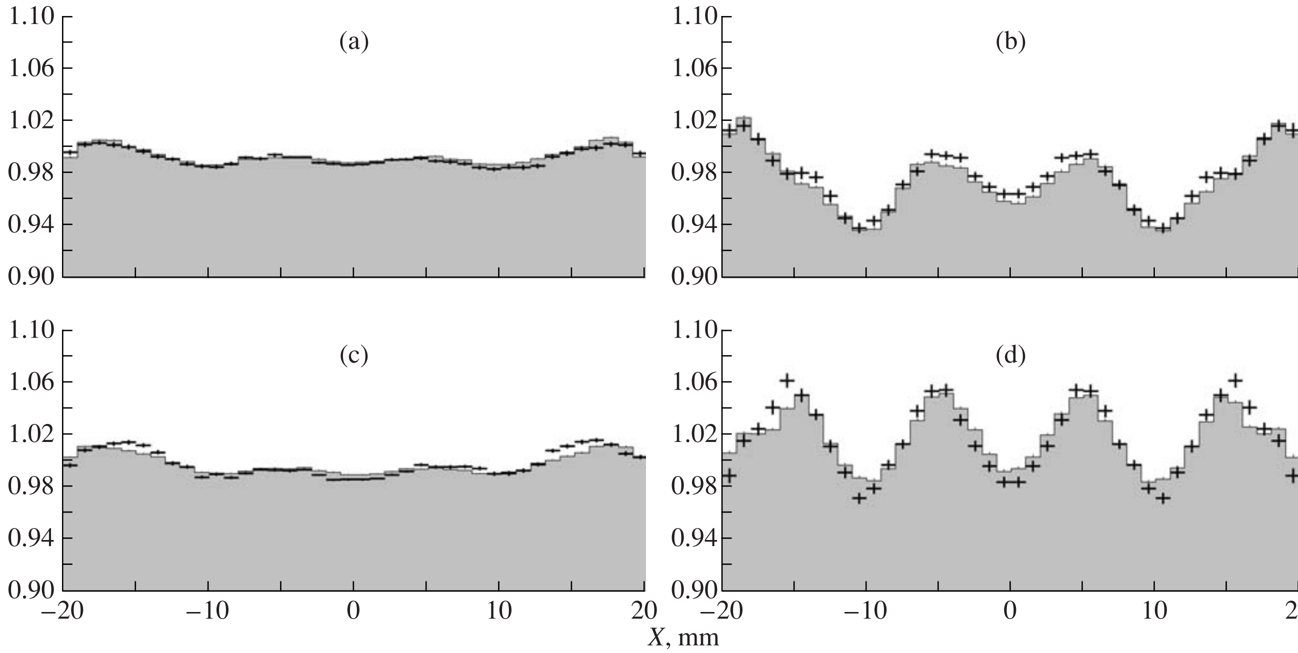

Fig. 10. Nonuniformity of the response of the LHCb inner module (a, c) to electrons and (b, d) to muons, measured (dots) and simulated (a histogram) (a, b) between fibers and (c, d) near the fibers.

Several slices of the two-dimensional normalized model map of the nonuniformity in the inner module of the LHCb calorimeter for high-energy muons and 5-GeV electrons are presented in Fig. 10; the experimental data are also plotted in this figure. The histograms in Figs. 10a and 10b correspond to slices between the fibers; those in Fig. 10c and 10d correspond to the regions near the fibers. It is apparent that the model truly describes the experimental data. The variation in the calorimeter response to electrons is much smaller than that to muons. For electrons, the nonuniformities of the colorimeter response are effectively averaged over the surface of the sensitive cell in accordance with the transverse profile of electromagnetic shower development.

A large width of electromagnetic showers is also the cause of the differences in behavior of the calorimeter response curves at the edges of the light-isolated cell. For electrons, some energy of an electromagnetic shower is lost in the dead material between light-isolated cells of the module. These losses are compensated for by an increase in the light collection efficiency near the edges of the tile owing to diffuse reflection of light from the matte coating of the border and end surfaces of the tile (see Section 5). In histograms presented in Figs. 10c and 10d, one can easily discern maxima of the detector response near the WLS fibers. For verification, the nonuniformity maps of the inner module response to 100-GeV muons were also simulated using the Geant4 transport code [3]. The nonuniformity maps obtained thereby coincided with the results of simulation based on the GEANT3 code.

The homogeneity of light collection in the middle modules of the LHCb calorimeter did not virtually differ from the homogeneity measured in the inner modules, since the distance between the WLS fibers in these modules was the same. The results of simulation and the experimental data for the muon scan of the outer module of the LHCb calorimeter are presented in Fig. 11. Two delay wire chambers only were used to acquire these data, thus making it impossible to reject inaccurately reconstructed tracks. Therefore, the light collection uniformity curve measured with the outer module was additionally smeared, since the accuracy in determining the coordinates of the point of incidence on the calorimeter module was significantly worse (0.5 mm). This smearing was also taken into account in the GEANT simulation of the detector response. The histogram in Fig. 11a corresponds to the slice of the histogram between the fibers, while the histogram in Fig. 11b corresponds to the slice near the fibers. The higher nonuniformity of the outer module’s response as compared to that of the inner module is explained by the larger spacing between the fibers of the outer module (15 mm).

Several slices of the two-dimensional normalized model map of the nonuniformity in the experimental module are shown in Fig. 12; the experimental data are also plotted in this figure. A sharp increase in the nonuniformity of the experimental module’s response in comparison with the inner module of the LHCb calorimeter was caused by the small thickness of the scintillator tiles. The effect that the tile thickness has on the homogeneity of light collection is described in detail in

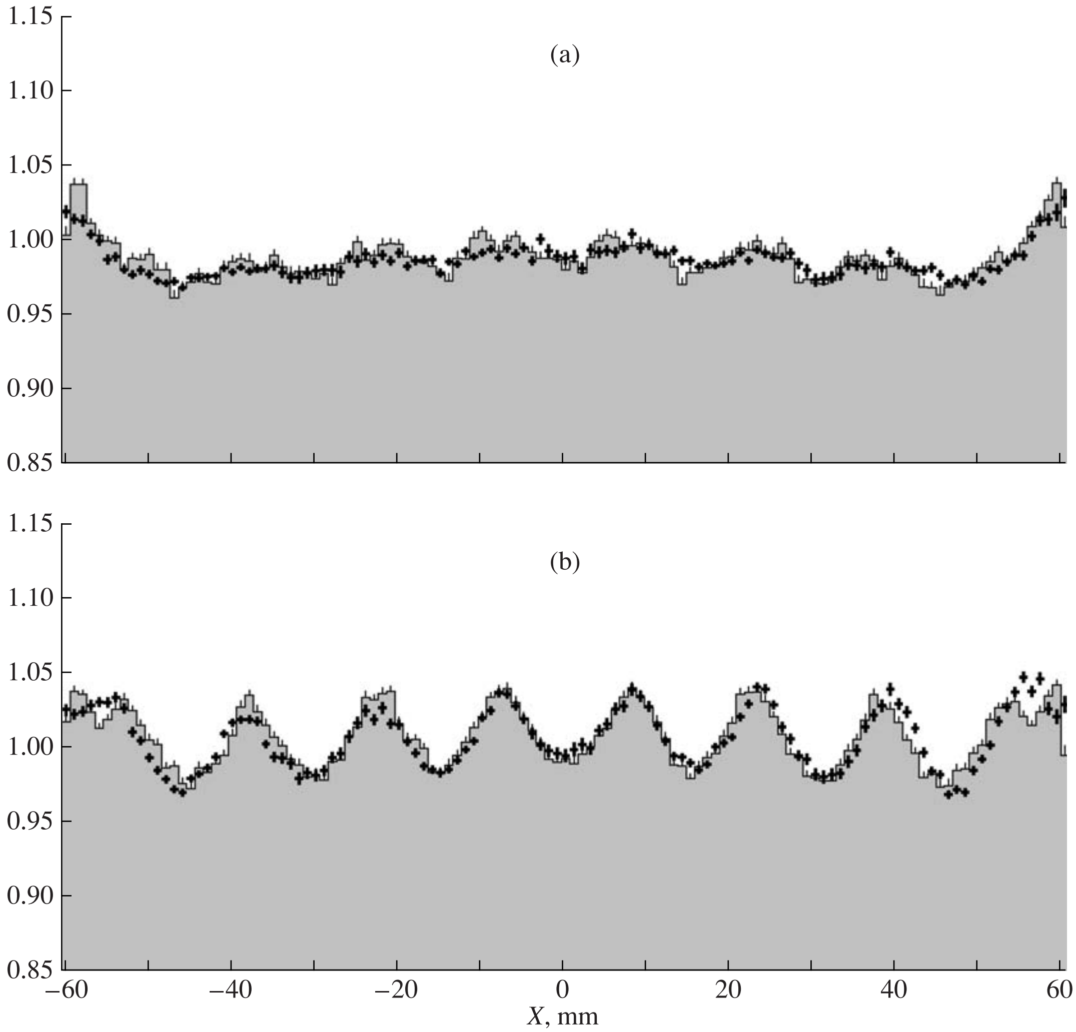

Fig. 11. Nonuniformity of the response of the LHCb outer module to muons: (a) slices of the histograms with averaging over a width of 2 mm between fibers and (b) a similar slices near fibers; dots correspond to the experimental data, and a histogram presents the simulation results.

Section 5. The edges of the scintillator tiles used in the experimental module did not have a border of matte coating; this fact provides an explanation for the behavior of the detector response at the edges. For all distributions presented, the χ^2 value (per degree of freedom) is in the range of 2–4, which is explained by the individual features of the measured modules, taking account of which in our simulation is extremely difficult and falls beyond the scope of our study.

The dependence of the calorimeter response nonuniformity on the quality of matte coating, the surface condition of the scintillator, its refractive index, the attenuation length in the tiles, and other factors was investigated. The first two parameters were found to exert the strongest effect on the results of simulation. The values of these parameters, determined from comparison with the experimental data, are summarized in Table 3. Variations within reasonable limits (e.g., for the refractive index of the scintillator, we analyzed the values of 1.52–1.62; for the decay length in a tile, 100–400 mm) of the other parameters affect the homogeneity of light collection only slightly.

The developed model of the scintillator tile with parameters determined from the experimental data was used to predict the relative light yield in all tested modules. The results obtained were normalized to the number of photoelectrons per 1 GeV of the bombarding electron energy, measured during the beam tests of the inner LHCb module. The results of simulation are presented in Table 2 in comparison with the experimental data obtained in the course of beam tests and measurements on the test bench with the use of cosmic rays.

5. DISCUSSION OF RESULTS

The nonuniformity of light collection can be divided into local and global nonuniformities. The global nonuniformity results from the nonzero probability of light

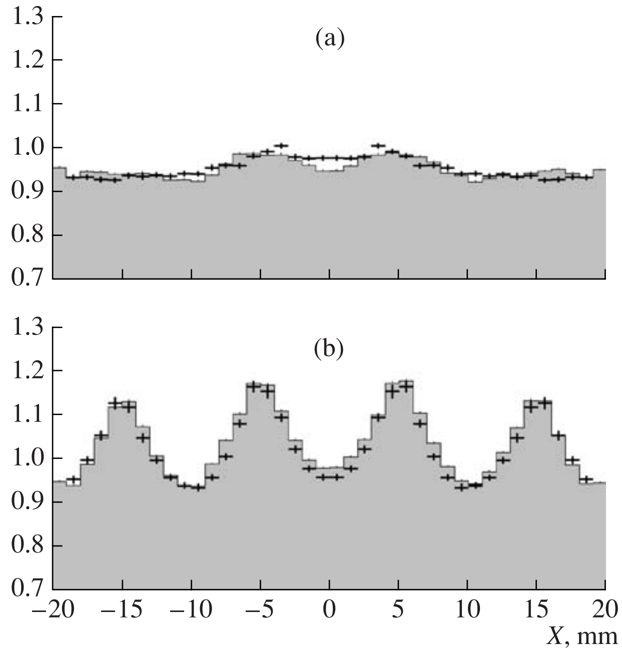

Fig. 12. Nonuniformity of the response of the experimental module to muons: (a) slice averaged over a width of 1 mm between fibers and (b) a similar slice near fibers; dots correspond to the experimental data, and a histogram shows the simulation results.

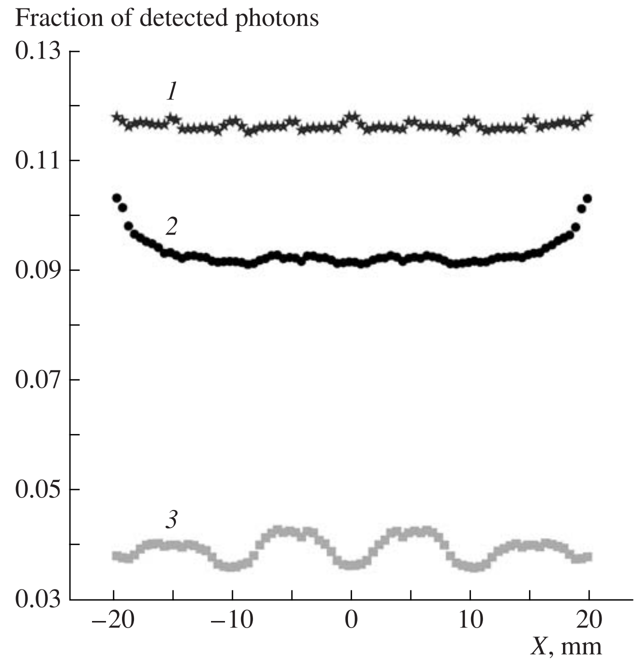

Fig. 13. Results of simulation of the light collection efficiency between fibers for a tile (*1*) with end surfaces providing perfect mirror reflection, (*2*) end surfaces providing diffuse reflection, and (*3*) transparent end surfaces.

being absorbed at the end surfaces of the tile and an increase in the light collection efficiency at the tile edges. The latter is caused by the diffuse character of reflection from the matte coating of the end surfaces and the border. In fact, if we assume that there is a perfectly reflecting mirror at the end surfaces of the scintillator tile, the difference between its edges and center disappears (curve *1* in Fig. 13). In a qualitative sense, diffuse reflection from the end surfaces and the border means that a photon produced near the tile edge directly under the white border and moving along a vertical line will change its direction and, possibly, fly inside the tile, suffering a sequence of total internal reflections. Should the matte coating be absent, there is a high probability that such a photon will escape from the tile and be absorbed. An increase in the light collection efficiency at the edges of tiles must compensate for the presence of a dead material between them. Exact compensation may be achieved by changing both the quality of the matte coating at the end surfaces and border of the tile and the width of the border itself.

The local (i.e., interfibrillar) nonuniformity can be explained based on the following considerations. A major portion of photons is captured by fibers surrounding photon production points. The number of directly captured photons is highly dependent on the distance to the nearest fiber. It is this dependence that determines the interfibrillar nonuniformity (Fig. 14). The other photons propagate in the tile by total internal reflections and may cross the tile several times before being captured by any WLS fiber. The probability of such indirect capture is independent of the distance between the photon production point and the nearest fiber and slightly declines only in the vicinity of the fibers due to the screening effect (the nearest hole screens most of the other fibers from this photon). In thinner tiles, a photon must suffer more reflections from the upper and lower surfaces of the tile in order to travel the same distance in a horizontal plane. Since there is a

Table 3. Main optical parameters of the scintillator tile model

Optical parameters	Inner module		Outer module. Muons	Experimental module. Muons
	muons	electrons		
Quality of the matte coating	1.13 ± 0.02	1.14 ± 0.02	1.12 ± 0.02	1.13 ± 0.02
Surface imperfection	0.06 ± 0.01	0.06 ± 0.01	0.06 ± 0.01	0.06 ± 0.004

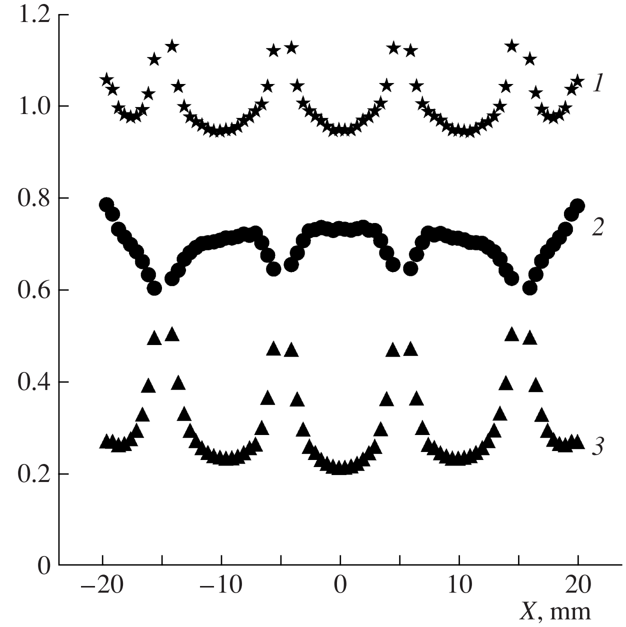

Fig. 14. Simulated efficiency of light collection by the fibers: (*1*) photons absorbed by four fibers closest to the photon production point, (*2*) photons absorbed by the other fibers, and (*3*) total nonuniformity.

nonzero probability that a photon will be absorbed after being reflected, a fraction of indirect photon capture decreases with a decrease in the tile thickness, while the local nonuniformity increases.

6. CONCLUSIONS

In the course of beam tests of the LHCb calorimeter modules and the experimental module having 0.5-mm-thick lead and scintillator plates, the nonuniformity of their responses to 50-GeV electrons and 100-GeV muons was measured. The light yield in these modules was determined. A program simulating light collection inside scintillator tiles of the calorimeter was developed. Optical models of the scintillator tiles of the outer, middle, and inner modules of the LHCb calorimeter and the experimental module with 0.5-mm-thick lead and scintillator plates were constructed. The parameters of the optical model were determined by comparing the results of simulation to the experimental data. The simulation results are seen to adequately describe the data obtained. The model data on the light yield are shown to coincide with the experimental results.

The measured nonuniformity of the response of the electromagnetic calorimeter modules are necessary for correct simulation of the detector response and must be taken into account in particle reconstruction algorithms in the LHCb experiment.

To reduce the nonuniformities (but not to completely eliminate them!) in thin scintillator tiles, first and foremost, the surface conditions of the scintillator must be improved, which will result in additional increase in the light yield, particularly in very thin tiles. Further increase in the homogeneity of the calorimeter response can be attained only by using additional methods, such as a method for forming light masks by applying paint to the surfaces of a scintillator tile and a Tyvek sheet.

ACKNOWLEDGMENTS

We thank K.R. Mikhailov for useful discussions.

REFERENCES

1. *LHCb Calorimeters Technical Design Report*, 2000, CERN/LHCC/2000-0036, LHCb TDR 2.
2. CERN Program Library Long Writeup W5013, 1993.
3. Agostinelli, S., Allison, J., Amako, K., et al., *Nucl. Instrum Methods Phys. Res. A*, 2003, vol. 506, p. 250.
4. Gatignon, L., *The West Experimental Area at the CERN SPS*, 2000, CERN-SL-2000-016-EA.
5. Spanggaard, J., *Delay Wire Chambers—a User Guide*, 1998, CERN-SL-98-023-BI.
6. Yao, W.-M., Amsler, C., Asner, D., et al., *J. Phys.*, 2006, vol. G 33, p. 1.
7. *LHC Computing Grid—Technical Design Report*, 2005, LCG-TRD-001 CERN-LHCC-2005-024.
8. Brun, R. and Rademakers, F., root.cern.ch.